Journal of
Synchrotron
Radiation

ISSN 0909-0495

Received 7 April 2011
Accepted 8 July 2011

Measurement of angular distribution of soft X-ray radiation from thin targets in the tabletop storage ring MIRRORCLE-20SX

Hironari Yamada,[a,b]* Dorian Minkov,[b] Yuki Shimura,[b] Chris Scourtis,[c] Okoye Kenneth Ejike,[b] Daisuke Hasegawa,[a] Mami Yamada,[a] Takayasu Hanashima[a] and Ken Atkinson[c]

[a]Photon Production Laboratory Ltd, 4-2-1 (808) Omihachiman, Shiga, Japan, [b]Synchrotron Light Life Science Centre, Ritsumeikan University, Shiga, Japan, and [c]CSIRO Materials Science and Engineering, Belmont, Australia. E-mail: hy@se.ritsumei.ac.jp

The only available tabletop electron storage rings are the machines from the MIRRORCLE series. The electrons are accelerated in a microtron and injected into the storage ring. During its circulation, each electron passes through a tiny target many times, emitting a photon beam. Both the spectrum and the angular distribution of the radiation depend on the material, the thickness and the shape of the target. In this paper measured angular distributions of the radiation from several different targets in the magnetic field of the 20 MeV storage ring MIRRORCLE-20SX are presented. The detector comprises a 3 mm × 3 mm × 8.5 μm plastic scintillator (PS) coupled to a photomultiplier by a bundle of optical fibers. The output of the photomultiplier is digitized by an IF converter. This detector is sensitive mostly to soft X-ray radiation, and its PS is moved by a mechanical system in a plane perpendicular to the radiation axis. The measured angular distributions for Mo and Sn targets contain an annulus which is attributed to transition radiation. The angular distributions for Al, carbon nanotube and diamond-like carbon (DLC) targets show some suppression of the radiation along the magnetic field. This is the first evidence of observation of the angular distribution of synchrotron Cherenkov radiation, which represents Cherenkov radiation in a magnetic field. The power radiated from the DLC target is estimated.

Keywords: tabletop storage ring; target; angular distribution; synchrotron Cherenkov radiation; Cherenkov radiation; transition radiation.

1. Introduction

Among the variety of accelerators, storage rings are used in applications requiring high-power radiation (Krinsky *et al.*, 1983; http://www-ssrl.slac.stanford.edu/; Bryant & Johnsen, 1993). Almost all storage rings are huge public property machines, fixed at distant places, which impedes their use.

The only available tabletop storage rings are those from the MIRRORCLE series. They include machines operating with 1, 4, 6 and 20 MeV electrons (Yamada, 1994; http://www.photon-production.co.jp/). During its circulation in the storage ring, each relativistic electron passes through a small target many times, emitting a photon beam (Fig. 1). The radiation spectrum depends on the material and the geometry of the target. The possible radiation mechanisms are bremsstrahlung, transition radiation and Cherenkov radiation (Jackson, 1999).

Bremsstrahlung (BS) has a wide spectrum, spreading up to the energy of the electrons (Koch & Motz, 1959; Yamada, 1996). Transition radiation (TR) has a narrower spectrum than bremsstrahlung, and its maximum spectral intensity can be located in the soft X-ray region, for a target made of light material with a thickness $d \simeq 1$ μm (Piestrup *et al.*, 1985; Yamada *et al.*, 2008). According to its general theory, TR

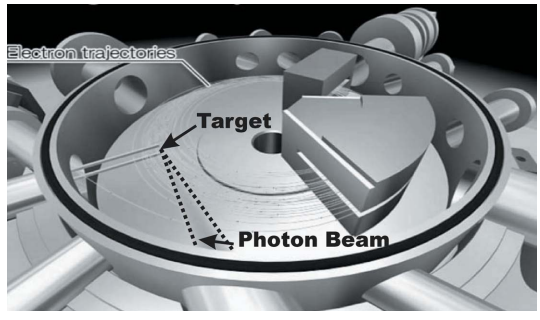

Figure 1
Each of the electrons circulating in MIRRORCLE passes through a small target many times, emitting a photon beam. The magnetic field is perpendicular to the circulation plane.

should be emitted in a hollow symmetrical cone with $\theta_{max} \cong \Delta\theta \simeq 1/\gamma$, where θ, $\Delta\theta$ and γ are the angle between the radiation axis and the emitted photon, the angular half-width of the radiation, and the relativistic factor, respectively (Piestrup *et al.*, 1991). In the X-ray region, Cherenkov radiation (CR) is radiated only when the real part χ' of the susceptibility of the target material is positive, which results in a narrow spectrum with a typical FWHM width of several electronvolts. According to its general theory, CR should be emitted at radiation angles $\theta = (\chi' - 1/\gamma^2)^{1/2}$ in a hollow symmetrical cone (Knulst *et al.*, 2003).

Concerning theoretical studies of the above radiation mechanisms for electrons in the presence of a magnetic field, we are aware only of work done on CR (Latal & Erber, 1977): this radiation mechanism has been named 'synchrotron Cherenkov radiation (SCR)' and its theory has been developed assuming that the radiation is emitted over the entire circular path of the electrons. Subsequent study has concluded that the angular distribution of SCR radiation shrinks somewhat towards the median plane (the circulation plane of the electrons) with respect to the hollow radiation cone for CR (Rynne *et al.*, 1978). In the only available experimental confirmation of the SCR theory (Bonin *et al.*, 1986), the dependence of the intensity of radiation from He gas in a magnetic field as a function of the gas pressure has been fitted best by calculated results based on the SCR theory.

In this paper measured angular distributions of radiation from several targets made of different materials in our storage ring MIRRORCLE-20SX are presented. Our aim was to account for the soft X-ray energy part of the radiation spectrum. The possible radiation mechanisms are discussed.

2. Experimental set-up

In the MIRRORCLE-20SX machine, electrons are accelerated to 20 MeV by a microtron and then injected, as ~200 ns pulses with up to 100 mA peak current and 400 Hz injection frequency, into the storage ring. There the electrons move along exactly circular orbits of radius 15 cm (Yamada, 1998, 2003). The magnetic field at the central orbit is about 0.4 T, the accumulated beam current is more than 3 A and the bunch length is ~20 mm (Haque *et al.*, 2009).

Our scheme for measuring the angular distribution of radiation from a target in MIRRORCLE is illustrated in Fig. 2. The injected peak electron current was I_p = 100 mA and the injection frequency was f = 70 Hz.

The targets were shaped as either one strip of width ~3 mm or one wire, and the target length was always 10 mm. Sn wire, Mo strip and Al strip targets were made of locally available materials. Diamond-like carbon (DLC) films were bought from TRIUMF in Canada and used for making our DLC strip target. Carbon nanotube (CNT) yarns were supplied courtesy of our collaborators from CSIRO, Australia, and utilized for our CNT yarn target. The five above-mentioned targets were mounted on their target holders in our laboratory. Each strip target was fixed in the storage ring so that the electron beam passed through a target area of about 3 mm × 3 mm. The long axis of each target was set to be parallel to the magnetic field of the storage ring.

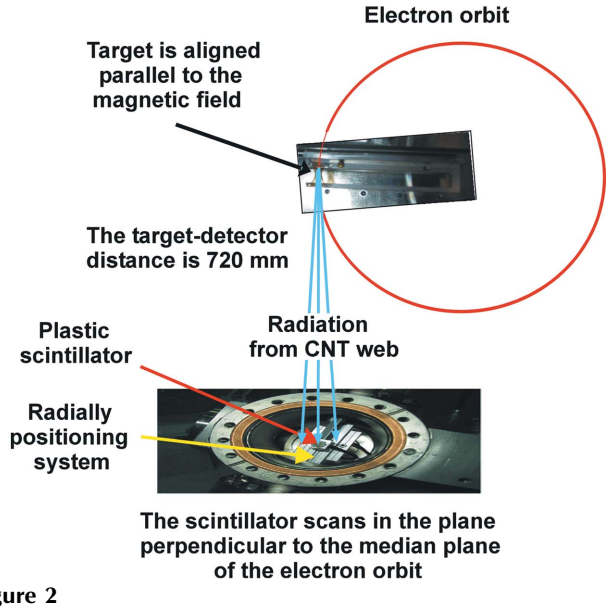

Figure 2
Scheme for measuring the angular distribution of the radiation. A strip or wire target is fixed parallel to the magnetic field of the storage ring. A plastic scintillator (PS) is mounted in the vacuum chamber, while the flange axis coincides with the radiation axis. The PS is rotated around that axis in 22.5° steps, and also moved radially away from the axis, up to 36 mm, with a step of 4 mm.

The detector included an 8.5 µm-thick and 3 mm × 3 mm square plastic scintillator (PS) coupled to a H3165-10 photomultiplier (PM) of Hamamatsu Photonics, operated at 1 kV, by a bundle of optical fibres. The output current of the photomultiplier was digitized by an IF converter, the readout of which was in units of 10^{-10} A. This detector was calibrated using a synchrotron source from 30 eV to 1170 eV, and the spectral dependence of its efficiency is shown in Fig. 3.

To measure the angular distribution of the radiation, we scanned the radiation field by rotating the PS 360° around the radiation axis in steps of 22.5°, and then changing the radial

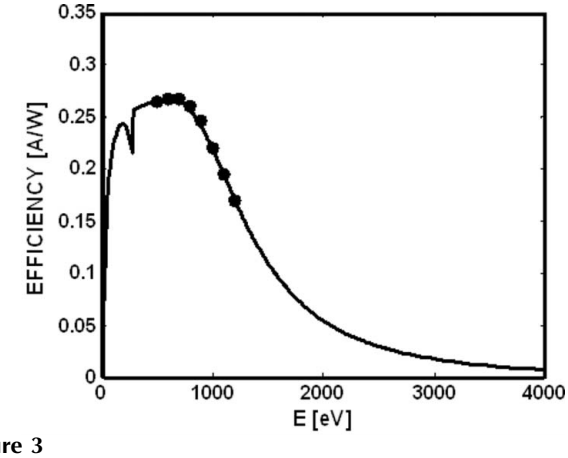

Figure 3
Spectral dependence of the efficiency of the detector. Circles: calibrated data; line: our analytical approximation of these data. The detector includes a 8.5 µm-thick NE102 plastic scintillator, an optical bundle of diameter 6 mm, and a H3165-10 photomultiplier operated at 1 kV.

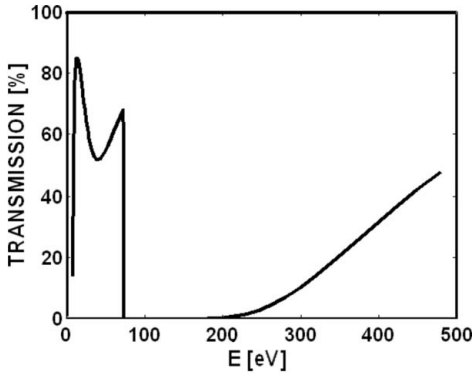

Figure 4
Calculated spectral dependence of the transmission of radiation through the 385 nm-thick Al filter.

distance from zero to 36 mm with a step of 4 mm. The radiation axis was along the direction of the electron beam crossing the target. The PS-scanned plane *XY* was located at 720 mm from the target.

In one of our experiments a 385 nm-thick Al filter was fixed between the target and the detector. The spectral dependence of the transmission of radiation through this filter was calculated using the NIST database (http://physics.nist.gov/PhysRefData/FFast/html/form.html), and the result is presented in Fig. 4. To validate this filter, we performed a light transmission experiment using an EUV lamp and the PS-based detector, which showed that less than 0.1% of that EUV radiation had passed through the filter.

3. Experimental results

The measured angular distribution of the radiation from each target is illustrated by both two-dimensional and three-dimensional graphs. The point 0 of the PS-scanned plane *XY* is the place where straight radiation from the target hits this plane. The *X*-axis is in the median plane of the ring, and the *Y*-axis is parallel to the magnetic field. The *Z*-axis gives the number of counts at the detector output. Each two-dimensional graph represents a top view of its respective three-dimenisonal graph.

3.1. Results for heavier-element targets

The measured angular distribution of the radiation from a 5 µm-thick Mo strip target is shown in Fig. 5. The angular distribution for Sn wire with a diameter of 150 µm is presented in Fig. 6. In both cases annular-type angular distributions are observed, and the annulus is wider for the Sn target. The average angular spread of the annuli for the Mo target and the Sn target is about 14 mrad, while the annulus width is ∼11 mrad for the Mo target and ∼22 mrad for the Sn target.

3.2. Results for lighter-element targets

The angular distribution for a 385 nm-thick Al strip target is shown in Fig. 7. Fig. 8 illustrates the result for CNT yarn with a diameter of 15 µm.

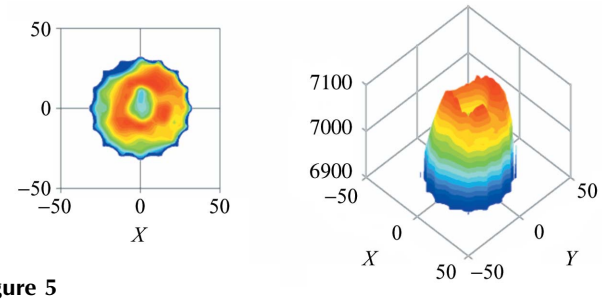

Figure 5
Measured angular distribution of the radiation from the 5 µm-thick Mo strip target.

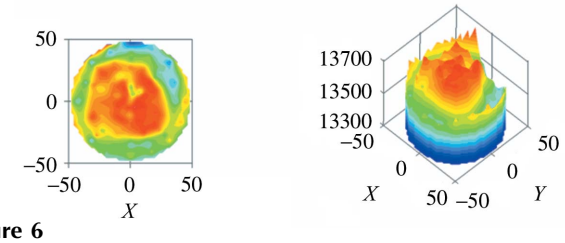

Figure 6
Angular distribution for Sn wire of diameter 150 µm.

The angular distribution of the radiation from a 55 nm-thick DLC strip target was measured twice, while a 385 nm-thick Al filter was fixed in front of the PS during the second measurement. Three angular distributions are shown in Fig. 9 for this target: without Al filter, with Al filter, and the difference between these two distributions.

The measured angular distributions for lighter-element targets are different from those for heavier-element targets. Essentially, two spots are observed close to the *X*-axis, which is perpendicular to the magnetic field, for all of the investigated lighter-element targets without a filter. The separation

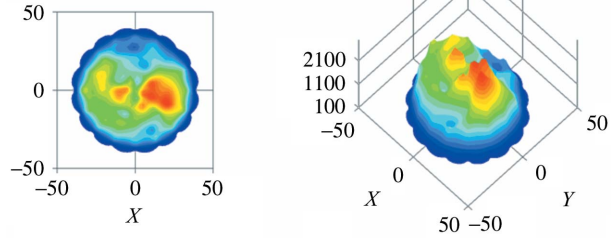

Figure 7
Angular distribution for the 385 nm-thick Al strip target.

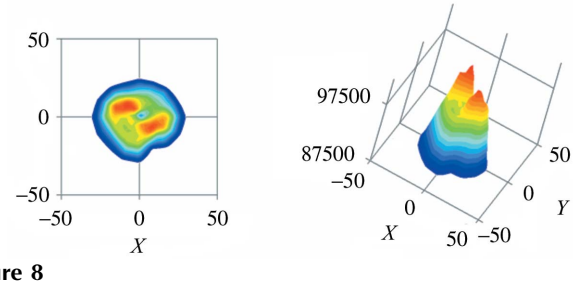

Figure 8
Angular distribution for the CNT yarn with a diameter of 15 µm.

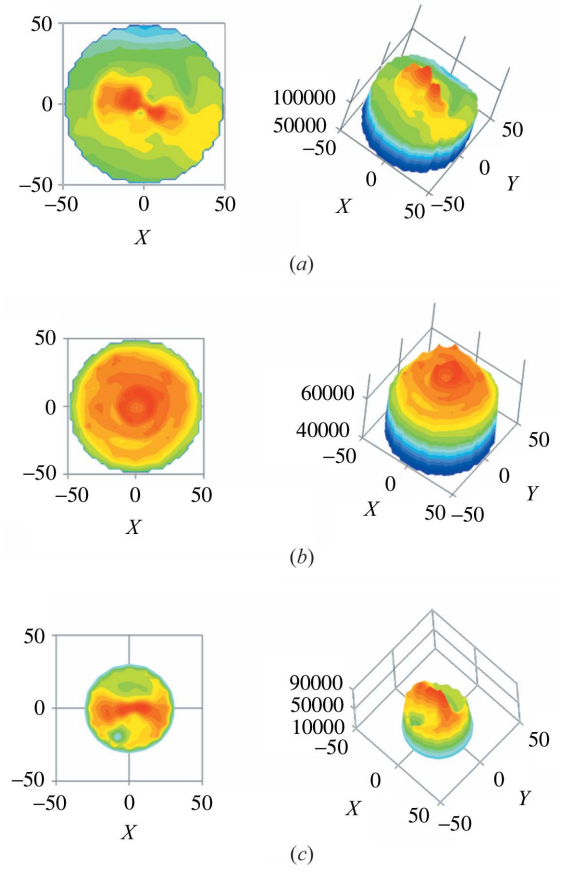

Figure 9
Angular distributions of the radiation from the 55 nm-thick DLC strip target. (*a*) Without Al filter. (*b*) With a 385 nm-thick Al filter in front of the PS. (*c*) The difference between the above two distributions.

between the two spots is only ∼20 mrad for the CNT target.

In the measurement for the DLC target with Al filter in front of the PS, an annular-type angular distribution is observed, similar to those for the heavier-element targets. The ∼8 mrad average angular spread is smaller than that for the heavier-element targets.

4. Discussion of the experimental results

To estimate the role of visible light in our experimental results, we calculated the output currents attributed to visible and soft X-ray TR radiation. These results are shown in Appendix *A*, and they indicate that the contribution of visible light to our measured output currents is negligible. Also, the small detector outputs in another experiment without a target indicate that the contribution of synchrotron radiation in MIRRORCLE is negligible.

In our previous quantitative study of radiation from thin targets in the 6 MeV storage ring MIRRORCLE-6X, we found that the contribution of BR to our 6 MeV angular distributions was relatively small because our detector is sensitive predominantly in the soft X-ray energy spectral region (Toyosugi *et al.*, 2007). Here we calculated the relative contributions of BS and TR to the output currents data for the DLC strip target with Al filter, shown in Fig. 9(*b*). These results are presented in Appendix *B* and they show that the contribution of BR is significantly smaller with respect to TR for the DLC target with Al filter.

In the study of Toyosugi *et al.* (2007), two radiation peaks were observed by scanning the radiation field only along the *X*-axis. That experimental procedure has now been upgraded, allowing angular distribution in the *XY* plane to be obtained. We observe an annular angular distribution for heavier-element targets, and both annular and two-spots-angular distribution for lighter-element targets. These angular distributions should have TR or CR origin.

CR is generated only when the real part of the susceptibility χ' is positive. In the soft X-ray region though, χ' is negative for Mo and Sn, according to the Henke database (http://physics.nist.gov/PhysRefData/FFast/html/form.html), which prohibits CR. Therefore, the annuli observed for the heavier-element targets should have TR origin.

The annulus for the Sn wire target is wider than that for the Mo strip target. This is associated with TR influenced by the different distances which the electrons pass through the wire (Piestrup *et al.*, 1985). The angular distribution for the Al-filtered DLC target also contains an annulus. This is a result of TR, since CR at the C edge is strongly absorbed by the Al filter, as seen from Fig. 4. The average angular spread of the annuli observed for the Mo target, the Sn target and the Al-filtered DLC target are smaller than $1/\gamma \simeq 24.9$ mrad, which is ascribed to a relatively larger contribution of higher-energy photons (Piestrup *et al.*, 1991). An estimation of the power radiated from the DLC target is presented in Appendix *C*.

Unlike for the heavy-element targets, the angular distributions for the lighter-element targets, without a filter, are characterized by two spots, which indicates some suppression of the radiation in the direction of the magnetic field. This is in a qualitative agreement with the theory of SCR (Rynne *et al.*, 1978), which predicts some suppression of the radiation along the magnetic field. Indeed, CR should be observed close to the *L*-edge of Al at 73 eV, and the *K*-edge of C at 284 eV (http://physics.nist.gov/PhysRefData/FFast/html/form.html). Our discussions with T. Erber confirmed that the angular distributions observed here for Al, CNT and DLC targets represent the first experimental evidence for angular distribution owing to SCR.

APPENDIX *A*
Estimating the contributions of soft X-ray and visible light to the measured output currents

The measured current I at the PM output is expressed as

$$I\,[\mathrm{A}] = N_{\mathrm{el/s}}\,[\mathrm{s}^{-1}]\,\Omega_{\mathrm{PS}} \int_E \frac{\mathrm{d}^2N}{\mathrm{d}E\,\mathrm{d}\Omega_{|\Omega_M}} E\,[\mathrm{eV}] \times 1.6022 \times 10^{-19}\, T_{\mathrm{rg}} S_{\mathrm{D}}\,[\mathrm{A\,W}^{-1}]\,\mathrm{d}E, \quad (1)$$

where $N_{\mathrm{el/s}}$ is the number of relativistic electrons passing through the target for 1 s, Ω_{PS} is the spatial angle over which the target irradiates the PS, $\mathrm{d}^2N/\mathrm{d}E\,\mathrm{d}\Omega_{|\Omega_M} = Y$ is the angular

Table 1
Calculated values of the angular spectral yield Y and the product YE of the angular spectral yield and the photon energy.

These data are for TR of 2 eV and 200 eV photons, and some of our target materials.

	Y(Mo)	Y(Sn)	Y(DLC)	Y(Mo) × E (eV)	Y(Sn) × E (eV)	Y(DLC) × E (eV)
2 eV	0.703	0.703	0.703	1.406	1.406	1.406
200 eV	0.00728	0.00680	0.00738	1.456	1.360	1.476

spectral yield, E is the photon energy, T_{rg} is the transmission through the residual gas in the storage ring, and S_D is the sensitivity of the detector. Calculated values of Y and the product YE [eV] are presented in Table 1 for TR from several of our target materials.

It is seen that the product YE has similar values for visible photons with E = 2 eV and photons with E = 200 eV for each of the three investigated materials. An analytical expression for the spectral dependence of our detector sensitivity S is derived by Toyosugi *et al.* (2007) based on calibrated data, which gives: S_D [2eV] $\simeq$ 0.079 and S_D [200 eV] $\simeq$ 0.24. Furthermore, visible TR is generated within only $\sim$3 eV bandwidth compared with $\sim$1500 eV bandwidth for soft X-ray TR. Therefore, an overview of (1) indicates that the contribution of visible light to our measured output currents is negligible.

APPENDIX *B*
Calculating the relative contributions of BS and TR to the output currents data for the DLC strip target with Al filter

The output current I_f for the DLC strip target with Al filter is

$$I_f\,[\mathrm{A}] = N_{\mathrm{el/s}}\,[\mathrm{s}^{-1}]\,\Omega_{PS}\int_E \frac{\mathrm{d}^2N}{\mathrm{d}E\,\mathrm{d}\Omega_{|\Omega_M}}\,E\,[\mathrm{eV}] \times 1.6022\times10^{-19}\,T_{rg}T_{Al}S_D\,[\mathrm{A\,W^{-1}}]\,\mathrm{d}E, \quad (2)$$

where T_{Al} is the transmission through the Al filter. Initially we calculated the spectral dependencies of the yields of TR and BR using formulae presented by Toyosugi *et al.* (2007). The contributions of TR and BR to the measured output current were calculated next from (2), which gave the ratio RTB = I_f(TR)/I_f(BS) between the output currents owing to TR and BS. The obtained results are: RTB(θ = 15 mrad) = 1388, and RTB(θ = 2 mrad) = 9.6. This shows that the angular distribution, shown in Fig. 9(*b*), for the DLC strip target with Al filter is predominantly due to TR, taking into account that SCR at the C *K*-edge is absorbed in the Al filter (see Fig. 4).

APPENDIX *C*
Estimation of the power radiated from the DLC target

Radiated power from the DLC target can be estimated by using the data from Fig. 9(*c*) and the calculation approach presented by Toyosugi *et al.* (2007), assuming that the radiation spectrum is relatively narrow, similar to CR at the *K*-edge of C. Since the output current for those data is proportional to the absorption of radiation in the Al filter, a maximum power of

$$\begin{aligned} P_{MAX} &= I_{MAX}/\left[(1-T_{Al})T_{rg}S_D\right](400/70)\\ &\cong 9.1\,[\mu A]/\left(0.925\times0.974\times0.2367\,[\mathrm{A\,W^{-1}}]\right)(400/70)\\ &\cong 244\,\mu W \end{aligned} \quad (3)$$

is radiated at full operational power of the storage ring with I_p = 100 mA and f = 400 Hz, within the solid angle Ω_{PS} = (3 × 3)/(720 × 720) = 1.74 × 10^{-5} sr, over which the target irradiates the PS, where I_{MAX} is the maximum measured current at the PM output, T_{Al} is the transmission through the Al filter, T_{rg} is the transmission through the residual gas in the storage ring, and S_D is the sensitivity of the detector from Fig. 3. The radiation brightness is P_{MAX}/Ω_{PS} = 244/1.74 × 10^{-5} μW sr^{-1} = 14 W sr^{-1}.

The total power P radiated at full operational power within the entire spatial angle $\Omega_M = 2\pi[1-\cos(\theta_M = 28.5\ \mathrm{mrad})] \simeq$ 0.00255 sr of the measured angular distribution is estimated by a summation over Ω_M, and

$$\begin{aligned} P &= I_{SUM}/\left\{(1-T_{Al})T_{rg}S_D\right\}(400/70)\\ &\cong 667.6.1\,[\mu A]/\left(0.925\times0.974\times0.2367\,[\mathrm{A\,W^{-1}}]\right)(400/70)\\ &\cong 17.9\,\mathrm{mW}. \end{aligned} \quad (4)$$

I_{SUM} represents a sum of data from Fig. 9(*c*) over Ω_M, where the number of addends is Ω_M/Ω_{PS}, while $P/\Omega_M \simeq$ 7 W sr^{-1}. The maximal brilliance of the radiation source is $P_{MAX}/(\Omega_{PS}S_R) \simeq$ 1.56 MW (sr m^2)$^{-1}$, and the brilliance for the entire spatial angle is $P/(\Omega_M S_R) \simeq$ 0.78 MW (sr m^2)$^{-1}$, where $S_R \simeq$ 3 mm × 3 mm is the radiating area.

References

Bonin, K. D., McDonald, K. T., Russell, D. P. & Flanz, J. B. (1986). *Phys. Rev. Lett.* **57**, 2264–2267.

Bryant, P. J. & Johnsen, K. (1993). *The Principles of Circular Accelerators and Storage Rings*, pp. 11–13. Cambridge University Press.

Jackson, J. D. (1999). *Classical Electrodynamics*, 2nd ed., pp. 647–714. New Jersey: John Wiley and Sons.

Knulst, W., van der Wiel, M. J., Luiten, O. J. & Verhoeven, J. (2003). *Appl. Phys. Lett.* **83**, 4050–4052.

Koch, H. W. & Motz, J. W. (1959). *Rev. Mod. Phys.* **31**, 920–955.

Krinsky, S., Perlman, M. L. & Watson, R. E. (1983). *Handbook on Synchrotron Radiation*, Vol. 1, pp. 65–74. New York: North-Holland.

Latal, H. G. & Erber, T. (1977). *Ann. Phys.* **108**, 408–442.

Monirul Haque, Md., Yamada, H., Moon, A. & Yamada, M. (2009). *J. Synchrotron Rad.* **16**, 299–306.

Piestrup, M. A., Boyers, D. G., Pincus, C. I., Harris, J. L., Maruyama, X. K., Bergstrom, J. C., Caplan, H. S., Silzer, R. M. & Skopik, D. M. (1991). *Phys. Rev. A*, **43**, 3653–3661.
Piestrup, M. A., Kephart, J. O., Park, H., Klein, R. K., Pantell, R. H., Ebert, P. J., Moran, M. J., Dahling, B. A. & Berman, B. L. (1985). *Phys. Rev. A*, **32**, 917–927.
Rynne, T. M., Baumgartner, G. B. & Erber, T. (1978). *J. Appl. Phys.* **49**, 2233–2240.
Toyosugi, N., Yamada, H., Minkov, D., Morita, M., Yamaguchi, T. & Imai, S. (2007). *J. Synchrotron Rad.* **14**, 212–218.
Yamada, H. (1994). *Asian Forum on Synchrotron Radiation*, edited by T. Ohta, S. Suga and S. Kikuta, pp. 17–18. Tokyo: Ionics Publishing.
Yamada, H. (1996). *Jpn. J. Appl. Phys.* **35**, L182–L185.
Yamada, H. (1998). *J. Synchrotron Rad.* **5**, 1326–1331.
Yamada, H. (2003). *Nucl. Instrum. Methods Phys. Res. B*, **199**, 509–516.
Yamada, H., Minkov, D., Toyosugi, N., Morita, M., Hasegawa, D., Moon, A. & Okoye, K. E. (2008). *J. Micro/Nanolithogr. MEMS MOEMS.* **7**, 043004.